A Reactant-Coordinate-Based Time-Dependent Wave Packet Method for Triatomic State-to-State Reaction Dynamics: Application to the H + O_2 Reaction†

Zhigang Sun,[‡,§] Xin Lin,[⊥] Soo-Y. Lee,[‡] and Dong H. Zhang*[,§]

Division of Physics & Applied Physics, School of Physical & Mathematical Sciences, Nanyang Technological University, Singapore 637371, State Key Laboratory of Molecular Reaction Dynamics and Center for Theoretical and Computational Chemistry, Dalian Institute of Chemical Physics, Chinese Academy of Sciences, Dalian 116023, People's Republic of China, and Department of Physics, The National University of Singapore, Singapore 119260

Received: November 30, 2008; Revised Manuscript Received: January 20, 2009

A new time-dependent wavepacket method is developed to study the A + BC → AB + C, AC + B reaction at the state-to-state level. The method only requires propagation of the wavepacket in reactant Jacobi coordinates by extracting *S*-matrix information on a dividing surface right before the absorption potential in the product region. It has particular advantages for reactions with deep wells and long-range attractive interactions in the product channels in which the wavepacket in the product channels can only be absorbed sufficiently far away from the interaction potential. Demonstration made on the benchmark H + H_2 reaction shows that the method is rather efficient in dealing with a direct reaction at high collision energy. The method is applied to study the very challenging H + O_2 ($v_0 = 0$, $j_0 = 0, 1$) reaction, with state-to-state differential cross sections obtained for the first time for collision energies up to 1.1 eV. The calculations not only show the power and accuracy of the new approach in dealing with complex-forming reactions but also shed light on the dynamics of the H + O_2 reaction.

1. Introduction

Following the establishment of quantum theory for atom−diatom reactive scattering in the 1970s,[1] significant progress has been made in the last two decades in quantum mechanical studies of dynamical chemical processes at the molecular level with the development of the hyperspherical-coordinate-based time-independent (TID) coupled-channel (CC) method[2−5] and the Jacobi-coordinate-based time-dependent wavepacket (TDWP) method.[6−17] The CC method has particular advantages in treating systems requiring a relatively small number of basis functions or systems with very low kinetic energy. It now can be routinely applied to study many triatomic reactions, such as H + H_2, F + H_2, and Cl + H_2 reactions and their isotopically substituted analogues,[18−24] and has provided great insights into chemical reaction dynamics. Recently, the TID method was applied to calculate fully converged state-to-state differential cross sections (DCS) for insertion reactions[5,25−27] and ion−molecule reactions[28] which are dominated by barrierless reactive pathways through deep wells and proceed via long-living complexes. The DCS achieved for these reactions have served as benchmarks for dynamics studies of complex formation reactions theoretically. However, due to the fact that the computational time in a CC calculation scales as N^3 (N is the number of basis functions), it is extremely hard to apply the CC method to study even more complex systems such as the H + O_2 reaction, which possesses a deep well and two heavy atoms other than hydrogen, despite some progress made recently.[29] The TDWP method scales much more favorably than the CC method in both memory and number of arithmetic operations; as a result, it is much more efficient in dealing with complex systems requiring a large number of basis functions. It has shown great power in calculating initial state-selected total reaction probabilities for systems involving more than three atoms by using reactant Jacobi coordinates.[12−14,16,17] However, to extract *S*-matrix elements in a TDWP calculation, one needs to transform the wave function initially prepared in reactant Jacobi coordinates to product Jacobi coordinates, making the calculations much more difficult.

Up to now, there were basically two main approaches to deal with the coordinate transformation problem for triatomic A + BC → AB + C, AC + B reactions. The first approach transforms the whole wavepacket from A + BC coordinates to AB + C/AC + B coordinates at a stage of propagation and obtains a scattering wave function for AB + C/AC + B channels after the propagation of the wavepacket in AB + C/AC + B coordinates.[8−11] The transformation can be made either when the wavepacket is at its initial asymptotic position[9−11] or after the initial "focusing" wavepacket is propagated into the interaction region.[8,30] This approach can be called the "product-coordinates-based" (PCB) approach because the main computation is carried out in product coordinates in that approach. For the PCB approach, it requires two separate main propagations to get *S*-matrix elements for both AB + C and AC + B channels. The second one is the well-known "reactant−product decoupling" (RPD) approach, which transforms the no-return part of the reacted wavepacket continuously in time from reactant to product coordinates with the help of absorption potentials.[31,32] The RPD approach is very efficient in dealing with direct reactants with barriers, as demonstrated by Althorpe and co-workers,[6,7] because, in this case, the absorption potential can be applied right after the barrier as in initial selected total reaction probability calculations, and it is also rather cheap to carry out the continuous propagation for the absorbed wave-

† Part of the "George C. Schatz Festschrift".

* To whom correspondence should be addressed. E-mail: zhangdh@dicp.ac.cn.

‡ Nanyang Technological University.

§ Chinese Academy of Sciences.

⊥ The National University of Singapore.

10.1021/jp810512j CCC: $40.75
Published on Web 02/26/2009

packet in a product channel. However, for a reaction with a deep well and a long-range attractive interaction in both the reactant and product channels, one has to put the absorption potential sufficiently far away to avoid absorbing the wave function, which may return into the deep well due to the long-range interaction, making the RPD approach less efficient. If there only exists a long-range attractive interaction in one product channel, which happens to be under investigation, the PCB method for that channel naturally becomes the right choice. However, for a reaction with a long-range attractive interaction in both product channels, the PCB method for one channel is not efficient anymore because of the long-range interaction in the other product channel. Therefore, neither the PCB or RPD method is efficient in dealing with a reaction with a long-range attractive interaction in both the reactant and product channels.

In this paper, we introduce a reactant-coordinate-based (RCB) wavepacket method to study the A + BC → AB + C, AC + B reaction at the state-to-state level using single reactant Jacobi coordinates. The method is complementary to the existing PCB and RPD methods and has particular advantages for reactions with deep wells and long-range attractive interactions in the product channels, in which the wavepacket in the product channels can only be absorbed sufficiently far away from the interaction potential. This means that in this case, the reacted wavepacket actually has almost reached the product asymptotic region before it is absorbed. Thus, one can obtain the scattering wave functions for both product channels in their corresponding asymptotic regions or the *S*-matrix elements for a state-to-state calculation by only propagating a wavepacket in reactant coordinates right before the wavepacket is absorbed. The key ingredient for the success of this method is to obtain the product scattering wave functions represented in the reactant channel basis efficiently. Dai and Zhang[33] once used a similar approach to get state-to-state reaction probabilities for the H + O_2 reaction for the total angular momentum $J = 0$ employing the time correlation function formalism for the *S*-matrix introduced by Tannor and Weeks.[34] As pointed out by the authors, the usage of the reactant Jacobi coordinate in their study was mainly due to the consideration for simplification in the TDWP propagation, not for the sake of optimal computational efficiency. Because they have to save the outgoing wavepacket for all interested product channels, it is impractical to extend this approach to $J > 0$ calculations due to the fact that the number of open channels increases almost linearly with J.

We will first show the application of the RCB method to the benchmark H + H_2 reaction and then show application of the method to the very challenging H + O_2 reaction. The H + O_2 → HO + O reaction is considered to be the single most important reaction in combustion chemistry.[35−38] Considerable amounts of experimental work have been carried out to measure the reaction rate coefficient and absolute cross sections. On the theoretical side, substantial effort has been devoted to developing a global PES for the HO_2 system from ab initio data. Among the existing PESs, the double many-body expansion (DMBE) IV PES of Varandas and co-workers[39] has been widely used in the past decade[40−48] because of its reasonable and balanced representation of the global properties of the PES. However, the accuracy of the DMBE IV PES has recently been questioned by several authors.[49−52] In 2005, Xu, Xie, Zhang, Lin, and Guo (XXZLG) reported a new PES for $HO_2(X^2A'')$ based on ~15000 symmetry-unique ab initio points obtained using the Davidson corrected internally contracted multireference configuration interaction method (icNRCI+Q) with a large (aug-cc-pVQZ) basis set.[53] Quantum studies on the new XXZLG PES demonstrated its high quality and uncovered many significant differences in spectroscopic and dynamic attributes from the DMBE IV PES.[54−58] Recently, Honvault et al. calculated DCS for the reaction near the reaction threshold by using the time-independent method.[29] Very recently, we briefly reported DCS for the reaction for collision energies up to 1.1 eV by using the RCB method.[59] Here, we present the details of the calculations and the results obtained.

The content of the paper is arranged as follows. In section 2, the basic theoretical aspects for extracting state-to-state cross sections using the RCB method are presented in detail. Section 3 presents the application of the method to the H + H_2 and the H + O_2 reactions; section 4 concludes the present work.

2. Theory

2.1. Reactant-Coordinate-Based (RCB) Approach. To study the A + BC → AB + C, AC + B reaction at a state-to-state level, we use three sets of body-fixed (BF) Jacobi coordinates to represent the corresponding wave functions, one for the reactant A + BC (denoted as the α arrangement), another for the product AB + C (denoted as the β arrangement), and the last for the product AC + B (denoted as the γ arrangement). Following the usual definition,[1,2] we write the coordinates as $(R_\nu, r_\nu, \theta_\nu; \mathbf{\Omega}_\nu)$, where ν is either α or β or γ. For $\nu = \alpha$ ($\nu = \beta, \gamma$), r_ν is the BC (AB, AC) bond length, R_ν is the length of the vector $\hat{R}_\nu$ pointing from A (C,B) to the BC (AB, AC) center of mass, and θ_ν is the angle between the BC (AB, AC) bond and $\hat{R}_\nu$; $\mathbf{\Omega}_\nu$ denotes the Euler angles orienting $\hat{R}_\nu$ in the space-fixed (SF) frame.

The basic idea for the RCB method is to propagate an initial wavepacket in the reactant Jacobi coordinates (α coordinates) as in an initial state-selected total reaction probability calculation to obtain scattering a wave function on the dividing surface for the β and γ product channels directly and efficiently right before the wavepacket is absorbed in the product region. In the present study, we implement it as follows:

(1) Select the dividing surfaces in product regions at $R_\beta = R_{\beta 0}$ and $R_\gamma = R_{\gamma 0}$, which should be as close as possible to the absorption potential but have no overlap with the absorption potential;

(2) On the dividing surfaces $R_{\nu 0}$ ($\nu = \beta,\gamma$), construct a potential optimized discrete variable representation (PODVR),[60] $r_{\nu i}$ ($i = 1,..., N_\nu^r$), and Gaussian−Legendre quadratures, $\theta_{\nu j}$ ($j = 1,..., N_\nu^\theta$), for r_ν and θ_ν, respectively, to represent scattering wave functions. Then, convert all of the grid points determined by $(R_{\nu 0}, r_{\nu i}, \theta_{\nu j})$ to their corresponding grid in reactant Jacobi coordinates

$$(R_{\alpha k}, r_{\alpha k}, \theta_{\alpha k}) = (R_\alpha(R_{\nu 0}, r_{\nu i}, \theta_{\nu j}), r_\alpha(R_{\nu 0}, r_{\nu i}, \theta_{\nu j}), \theta_\alpha(R_{\nu 0}, r_{\nu i}, \theta_{\nu j})) \quad (1)$$

where $k = 1,..., N_\beta^r \times N_\beta^\theta + N_\gamma^r \times N_\gamma^\theta$.

(3) Propagate the wavepacket as in an initial state-selected total reaction probability calculation and evaluate the time-dependent wave function on these grid points $(R_{\alpha k}, r_{\alpha k}, \theta_{\alpha k})$, from which the time-independent scattering wave functions can be obtained via a Fourier transform.

(4) Extract state-to-state *S*-matrix elements from the time-independent wave function by taking into account the residual long-range interaction, which we assume to only have an effect of elastic scattering in this study.

Because the representation of the chosen grid is very efficient, evaluation of the time-dependent wave function is carried out

on very limited grid points during the wavepacket propagation. As a result, the computational time for the evaluation step only takes about 20% of the total propagation time.

2.2. Wave Packet Representation in Reactant Jacobi Coordinates. The propagation of the wavepacket is only carried out in reactant Jacobi coordinates in the BF representation using the split operator method.[61,62] In reactant coordinates, the Hamiltonian for a given total angular momentum J can be written as

$$\hat{H} = -\frac{\hbar^2}{2\mu_{R_\alpha}}\frac{\partial^2}{\partial^2 R_\alpha} + \frac{(\boldsymbol{J}-\boldsymbol{j})^2}{2\mu_{R_\alpha}R_\alpha^2} + \frac{\boldsymbol{j}^2}{2\mu_{r_\alpha}r_\mu^2} + V(\boldsymbol{r}_\alpha,\boldsymbol{R}_\alpha) + \hat{h}(r_\alpha) \quad (2)$$

where μ_{R_α} is the reduced mass between the center of mass of A and BC, $\boldsymbol{J}$ is the total angular momentum operator, $\boldsymbol{j}$ is the rotational angular momentum operator of BC, and μ_{r_α} is the reduced mass of BC. The diatomic reference Hamiltonian is defined as

$$\hat{h}(r_\alpha) = -\frac{\hbar^2}{2\mu_{r_\alpha}}\frac{\partial^2}{\partial r_\alpha^2} + V_{r_\alpha}(r_\alpha) \quad (3)$$

where V_{r_α} is the diatomic reference potential.

The time-dependent wave function in the BF representation can be written as[63−66]

$$\Psi^{JM\epsilon}(\boldsymbol{R}_\alpha,\boldsymbol{r}_\alpha,t) = \sum_{K_\alpha}\mathscr{D}^{J\epsilon*}_{MK_\alpha}(\boldsymbol{\Omega}_\alpha)\psi_\alpha(t,R_\alpha,r_\alpha,\theta_\alpha;K_\alpha) \quad (4)$$

where $\mathscr{D}^{J\epsilon*}_{MK_\alpha}(\boldsymbol{\Omega}_\alpha)$ is the parity-adapted normalized rotation matrix, depending only on the Eular angles $\boldsymbol{\Omega}_\alpha$

$$\mathscr{D}^{J\epsilon*}_{MK_\alpha}(\boldsymbol{\Omega}_\alpha) = (1+\delta_{K_\alpha 0})^{-1/2}\sqrt{\frac{2J+1}{8\pi}} [D^{J*}_{MK_\alpha}(\boldsymbol{\Omega}_\alpha) + \epsilon(-1)^{J+K_\alpha}D^{J*}_{M-K_\alpha}(\boldsymbol{\Omega}_\alpha)] \quad (5)$$

where ϵ is the parity of the system defined as $\epsilon = (-1)^{j+l}$, with l being the orbital angular momentum quantum number, and $D^{J\epsilon}_{MK_\alpha}(\boldsymbol{\Omega}_\alpha)$ is the Wigner rotation matrix.[67] In eq 4, $\psi_\alpha(t,R_\alpha,r_\alpha,\theta_\alpha;K_\alpha)$, which only depends on three internal coordinates of the system and the projection of the total angular momentum K_α on the BF z axis (along $\boldsymbol{R}_\alpha$), can be expanded as

$$\psi_\alpha(t,R_\alpha,r_\alpha,\theta_\alpha;K_\alpha) = \sum_{n,v,j}F^{K_\alpha}_{nvj}(t)u^v_n(R_\alpha)\phi_v(r_\alpha)y_{jK_\alpha}(\theta_\alpha) \quad (6)$$

where n is the translational basis label, u^v_n is the translational basis function for R, which is dependent on v, as given in ref 41, $\phi_v(r_\alpha)$ is the eigenfunction for $\hat{h}(r_\alpha)$ given in eq 3, and $y_{jK_\alpha} = [(2j+1)/4\pi]^{1/2}d^j_{K_\alpha 0}$ are the spherical harmonics. The $d^j_{K_\alpha K_\nu}$ is a reduced Wigner rotational matrix[67] with $K_\nu = 0$.

2.3. Scattering Wave Function in the Product Region. To obtain time-independent scattering wave functions on the dividing surfaces in the product region, we first evaluate the time-dependent wave function given by eq 6 for every K_α component at all quadrature grid points $(R_{\nu 0},r_{\nu i},\theta_{\nu j})$ given in eq 1 at every time step

$$\psi(t,R_{\nu 0},r_{\nu i},\theta_{\nu j};K_\alpha) = \frac{R_{\nu 0}r_{\nu i}}{R_\alpha r_\alpha}\psi_\alpha[t,R_\alpha(R_{\nu 0},r_{\nu i},\theta_{\nu j}), r_\alpha(R_{\nu 0},r_{\nu i},\theta_{\nu j}),\theta_\alpha(R_{\nu 0},r_{\nu i},\theta_{\nu j});K_\alpha] \quad (7)$$

where $\nu = \beta, \gamma$ and hereafter indicates β or γ unless specified.

Then, we rotate the BF z axis from $\hat{R}_\alpha$ to $\hat{R}_\nu$ according to[1]

$$\psi_\nu(t,R_{\nu 0},r_{\nu i},\theta_{\nu j};K_\nu) = \sum_{K_\alpha}\psi(t,R_{\nu 0},r_{\nu i},\theta_{\nu j};K_\alpha)\times \frac{1}{\sqrt{(1+\delta_{K_\nu 0})(1+\delta_{K_\alpha 0})}}[d^J_{K_\nu K_\alpha}(\Delta) + \epsilon(-1)^{K_\alpha}d^J_{K_\nu -K_\alpha}(\Delta)] \quad (8)$$

where $d^J_{K_\nu K_\alpha}(\Delta)$ is a reduced Wigner rotational matrix[67] and Δ is the angle between $\hat{R}_\alpha$ and $\hat{R}_\nu$.

Finally, we expand $\psi_\nu(R_{\nu 0},r_{\nu i},\theta_{\nu j};K_\nu)$ in terms of basis functions for r_ν by the collocation method[32,68] and θ_ν by Gaussian−Legendre integration and combine it with $D^{J\epsilon*}_{MK_\nu}(\boldsymbol{\Omega}_\nu)$ shown in eq 5 to get the time-dependent wave function $R_\nu = R_{\nu 0}$

$$\Psi^{J\epsilon}_{v_\nu j_\nu K_\nu}(t;R_\nu = R_{\nu 0}) = \sum_{K_\nu}\mathscr{D}^{J\epsilon*}_{MK_\nu}(\boldsymbol{\Omega}_\nu)\sum_{v,j}C^{K_\nu}_{vj}(t)\phi_v(r_\nu)y_{jK_\nu}(\theta_\nu) \quad (9)$$

The energy resolved scattering wave function $\Phi^{J\epsilon}_{v_\nu j_\nu K_\nu}(E)$ in the BF coordinate can be obtained by a Fourier transformation

$$\Phi^{J\epsilon}_{v_\nu j_\nu K_\nu}(E;R_{\nu 0}) = \int_0^{+\infty}\mathrm{e}^{\mathrm{i}Et}\Psi^{J\epsilon}_{v_\nu j_\nu K_\nu}(t;R_{\nu 0})\mathrm{d}t \quad (10)$$

In practice, to reduce computational effort, one can first perform this Fourier transformation for ψ on the quadrature points shown in eq 7 and then carry out the BF z axis rotation and basis function expansion shown in eqs 8 and 9.

2.4. Initial Wave Packet and Extraction of the *S* Matrix. Practically, it is more convenient to construct an initial wavepacket and perform S-matrix extraction in the SF representation rather than in the BF representation as employed in some earlier studies,[6,9] although it is also possible to carry out these procedures in the BF representation without changing the locations of the initial wavepacket and the dividing surface to extract the S matrix. In the SF representation, an initial wavepacket for an initial state (v_0,j_0,l_0) can be constructed simply as

$$\Psi^{JM\epsilon}_{\alpha v_0 j_0 l_0}(t=0) = G(R_\alpha)\phi_{v_0 j_0}(r_\alpha)|JMj_0l_0\epsilon\rangle \quad (11)$$

where $|JMj_0l_0\epsilon\rangle$ is the total angular momentum eigenfunction in the SF representation with the parity of system $\epsilon = (-1)^{j_0+l_0}$, $\phi_{v_0 j_0}(r_\alpha)$ as the rovibrational eigenfunction for molecule BC and $G(R_\alpha)$ is a Gaussian wavepacket defined as

$$G(R_\alpha) = \left(\frac{2}{\pi\tau^2}\right)^{1/4}\exp\left[-\frac{(R_\alpha - R^c_\alpha)}{\tau^2} - \mathrm{i}k_cR_\alpha\right] \quad (12)$$

In order to propagate the wavepacket in the BF representation, one should transform $|JMj_0l_0\epsilon\rangle$ in eq 11 to its BF representation counterpart as[69]

$$|JMj_0l_0\rangle = \sum_{K_\alpha \geq 0} C^{Jj_0\epsilon}_{l_0K_\alpha}|JMj_0K_\alpha\rangle = \sum_{K_\alpha \geq 0} C^{Jj_0\epsilon}_{l_0K_\alpha}\mathscr{D}^{J\epsilon*}_{MK_\alpha}(\mathbf{\Omega}_\alpha)y_{j_0K_\alpha} \quad (13)$$

where $\mathbf{C}^{Jj_0\epsilon}_{l_0K}$ is the parity-adapted orthogonal transform matrix between the SF and BF representations[1,9,70−72] and is given by

$$C^{Jj\epsilon}_{lK} = \sqrt{\frac{(2l+1)}{(2J+1)}}\sqrt{(2-\delta_{K,0})}\langle jKl_0|JK\rangle \quad (14)$$

where $\langle ...\rangle$ is Clebsch−Gordan coefficient.

Similar to the construction of an initial wavepacket, the scattering wave function for an initial state $(v_0j_0l_0)$ in the BF representation $\Phi^{J\epsilon}_{v_\nu j_\nu K_\nu \leftarrow v_0 j_0 l_0}(E)$ in eq 10 is first transformed into the SF representation by the orthogonal transformation matrix given by eq 14

$$\Phi^{J\epsilon}_{v_\nu j_\nu l_\nu \leftarrow v_0 j_0 l_0}(E) = \sum_{K_\nu} C^{Jj_\nu\epsilon}_{l_\nu K_\nu}\Phi^{J\epsilon}_{v_\nu j_\nu K_\nu \leftarrow v_0 j_0 l_0}(E) \quad (15)$$

Then, the desired state-to-state scattering matrix $S^{J\epsilon}_{v_\nu j_\nu l_\nu \leftarrow v_0 j_0 l_0}(E)$ in the SF representation can be calculated from the asymptotic boundary condition

$$\Phi^{J\epsilon}_{v_\nu j_\nu l_\nu \leftarrow v_0 j_0 l_0}(E;R_{\nu 0}) = -\mathscr{A}(E)\left(\frac{2\pi\hbar^2 k_{v_\nu j_\nu}}{\mu_{R_\nu}}\right)^{1/2} S^{J\epsilon}_{v_\nu j_\nu l_\nu \leftarrow v_0 j_0 l_0}(E)\overline{\mathscr{H}}_{l_\nu}(k_{v_\nu j_\nu}R_{\nu_0}) \quad (16)$$

where $\mathscr{A}(E)$ is given by

$$\mathscr{A}(E) = \left(\frac{\mu_{R_\alpha}}{2\pi\hbar^2 k_{v_0 j_0}}\right)^{1/2}\int \overline{\mathscr{H}}_{l_0}(k_{v_0 j_0}R_\alpha)G(R_\alpha)\mathrm{d}R_\alpha \quad (17)$$

where $\overline{\mathscr{H}}_l$ is an outgoing Riccati−Hankel function.

Finally, the scattering matrix $S^J_{v_\nu j_\nu l_\nu \leftarrow v_0 j_0 l_0}$(E) in the SF representation is transformed into the helicity representation by the standard transformation

$$S^J_{v'j'K' \leftarrow vjK} = \sum_{l'l} i^{l-l'}\sqrt{\frac{2l'+1}{2J+1}}\langle j'K'l'_0|JK'\rangle S^J_{v'j'l' \leftarrow vjl}\sqrt{\frac{2l+1}{2J+1}}\langle jKl_0|JK\rangle \quad (18)$$

By substituting the scattering matrix $S^{J\epsilon}_{v_\nu j_\nu K_\nu \leftarrow v_0 j_0 K_0}(E)$ in the helicity representation into the standard formulas, the state-to-state integral cross sections[71] are then obtained

$$\sigma_{v_\nu j_\nu \leftarrow v_0 j_0} = \frac{\pi}{(2j_0+1)k^2_{v_0 j_0}}\sum_{K_\nu}\sum_{K_0}\sum_J (2J+1)|S^J_{v_\nu j_\nu K_\nu \leftarrow v_0 j_0 K_0}|^2 \quad (19)$$

and the state-to-state differential cross sections[71]

$$\frac{\mathrm{d}\sigma_{v_\nu j_\nu \leftarrow v_0 j_0}(\vartheta,E)}{\mathrm{d}\Omega} = \frac{1}{(2j_0+1)}\sum_{K_\nu}\sum_{K_0}\left|\frac{1}{2ik_{v_0 j_0}}\sum_J (2J+1)d^J_{K_\nu K_0}(\vartheta)S^J_{v_\nu j_\nu K_\nu \leftarrow v_0 j_0 K_0}\right|^2 \quad (20)$$

in which ϑ is the angle between the scattered AC + B/AB + C products and the incoming A + BC reactants.

2.5. Removing the Residual Long-Range Potential. At the dividing surface $R_\nu = R_{\nu 0}$, where the boundary condition matching that shown in eq 16 is carried out, the interaction potential between BC(AC) and A(B) should be negligibly small. For reactions with long-range interactions in the product region, this means that the value of $R_{\nu 0}$ should be sufficiently large, making the calculations in reactant Jacobi coordinates unfavorable. A simple way to reduce the value of $R_{\nu 0}$ is to include the elastic scattering effects after the dividing surface explicitly in the boundary condition, so that one can move the dividing surface to a place where inelastic scattering effects between BC(AC) and A(B) vanish. This can be achieved by replacing the outgoing Riccati−Hankel function in eq 16 by $\zeta_{vjl}(R)$, which satisfies the following equation

$$\left(-\frac{\hbar^2}{2\mu}\frac{\mathrm{d}^2}{\mathrm{d}R^2} + \frac{l(l+1)\hbar^2}{2\mu R^2} + U_{vjl}(R)\right)\zeta_{vjl}(R) = \frac{k^2_{vj}}{2\mu}\zeta_{vjl}(R) \quad (21)$$

where

$$\zeta_{vjl}(R) \sim \overline{\mathscr{H}}_l(k_{vj}R) \qquad \text{when} \quad U_{vjl}(R) = 0 \quad (22)$$

and $U_{vjl}(R)$ can be calculated as

$$U_{vjl}(R) = \langle\phi_{vj}|\langle JMjl\epsilon|V(R,r,\theta)|JMjl\epsilon\rangle|\phi_{vj}\rangle \quad (23)$$

with $V(R,r,\theta)$ being the residual long-range interaction, which should only have elastic effects after the dividing surface. The function $\zeta_{vjl}(R)$ can be simply obtained from eq 21 by backward propagating an outcoming Riccati−Hankel function from a place when $U_{vjl}(R) = 0$ by using the renormalized Numerov method.

We note that the similar method has been used by Launay and co-workers to take care of the long-range potential in ultracold triatomic collisions processes, except that they employed a finite difference method to solve eq 21.[73] In principle, by using this approach, we can reduce the value of $R_{\nu 0}$ further by including inelastic scattering effects from the residual long-range interaction after the dividing surface in the boundary condition. This will be pursued in our follow-up studies.

3. Results and Discussion

In this section, we will first present very briefly an application of the RCB method to the H+H_2 as a demonstration of the methodology. Greater details are then given for the application of the method to the H+O_2 reactions.

3.1. Application to the H + H_2 ($v_0 = 0, j_0 = 0$) Reaction. The H + H_2 exchange reaction and its isotopomers have been the focus of numerous experimental and theoretical studies. It is also a benchmark system for testing new theoretical methodologies. Aoiz et al. recently gave a comprehensive review on the progress on the dynamical study of this reaction.[74] With

advances in experimental and theoretical methods, excellent agreement between theory and experiment has been accomplished for this reaction on the BKMP2 potential energy surface (PES)[18,19,75,76] as well as on the latest CCI PES.[77,78] Here, we calculate DCS on the BKMP2 PES by using the RCB approach and compare the result with that obtained from the ABC program.[4]

The parameters used in the time-dependent wavepacket calculation are as follows. A total of 127 sine functions (among them, 59 for the interaction region) are employed for the translational coordinate R_α in a range of $[0.1,18.0]a_0$. A total of 69 vibrational functions are employed for r_α in the range of [0.5,11.6] for the reagent H_2 in the interaction region. We use $j_{max} = 60$ for the rotational basis. The permutation symmetry of the diatomic reagent is used, which saves half of the angular grid points. Calculations are carried out for J up to 42, with the maximum K value of 30 to converge the state-to-state differential cross sections for collision energies up to 2.5 eV. The time step used in the calculation is 15 au For low J partial waves, a total of 600 time steps are used to accomplish the wavepacket propagation from the reagent channel to the product channel. For higher J partial waves, the wavepackets are propagated for a shorter time because the reaction probability in the low energy range is negligible. Since the long-range interaction is small for this reaction, we can put the dividing surface at $R_{v0} = 7.0a_0$ to converge the state-to-state information without carrying out renormalized Numerov propagation after the dividing surface. For each K_α block, we use 8 PODVR points for r_v and 20 Gaussian−Legendre quadrature points for the rotational motion of the diatomic product. These 160 evaluation points are sufficient for obtaining all of the product-state-resolved information up to a collision energy of 2.5 eV.

It is worthwhile to point out that for a direct reaction with a barrier such as the H + H_2 reaction, the RCB method is less efficient than the RPD approach as one can see that the number of basis functions used here is substantially larger than that required in a RPD calculation. Nevertheless, our RCB calculation for the reaction is very fast even with such a large basis set. For $J = 0$, it only takes less than half of a minute of CPU time on a dual-processor work station.

Figure 1 shows the state-to-state DCS for some final states obtained by using our RCB approach at four collision energies. For collision energies of 0.76 and 1.36 eV, the DCS obtained using the ABC program[4] are also shown in Figure 1A−D for comparison. The parameters used for the ABC calculation are slightly larger than those used in the work of ref 11 with $K_{max} = 6$. It can be seen that the agreement for these two calculations is very good at these two collision energies, indicating that our RCB program is able to predict accurate DCS for triatomic reactions. However, to converge DCS at higher collision energies such as those shown in Figure 1E−H, we need to use a larger K_{max} for the ABC program, making it much more expensive than the RCB approach. Hence, the RCB method may be useful for studying direct triatomic reactions at higher collision energies.

3.2. Application to the H + O_2 ($v_0 = 0, j_0 = 0,1$) Reaction. In this subsection, we present the results for application of the RCB method to the endothermic H + O_2 ($v_0 = 0$, $j_0 = 0$, 1) reaction. The O_2 ($v_0 = 0$, $j_0 = 0$) molecule does not exist physically because of the nuclear spin statistics, but we can use it to test the numerical convergence of our calculations and to examine the influence of the reactant rotational state on reactivity. We use the XXZLG PES with a deep well (~2.38 eV from the H + O_2 asymptote), which supports long-lived

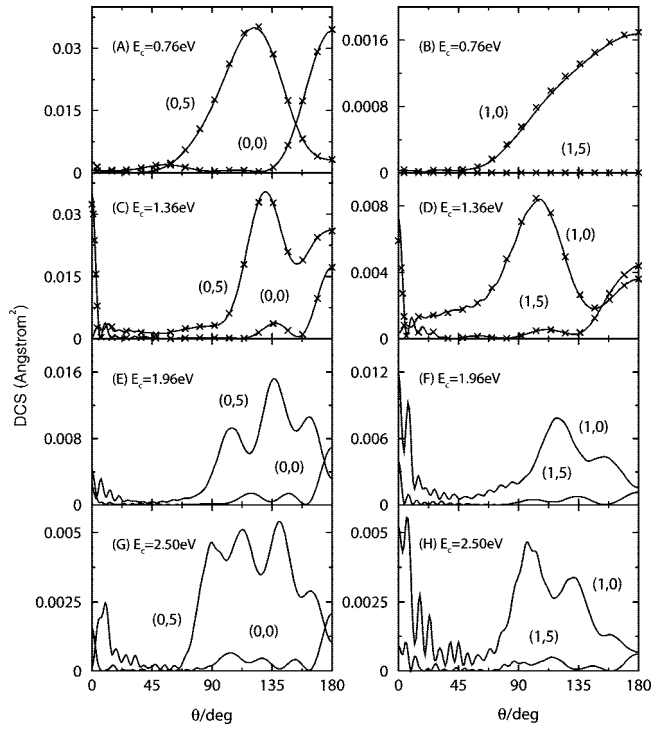

Figure 1. State-to-state DCS obtained by the RCB method (solid lines) for the H′ + H_2 ($v_0 = 0$, $j_0 = 0$) → H + HH′ ($v' = 0,1$, $j' = 0,5$) reaction at four selected collision energies. The DCS for $E_c = 0.76$ and 1.36 eV obtained by the ABC code are shown by the crosses for comparison.

resonances and has a long-range attractive interaction in the exit O + OH channel that requires a large grid size and long propagation time to accurately describe the sharp resonance peaks and the near-threshold energy reaction probabilities.[53] The numerical parameters used in the RCB calculations are as follows. A total of 235 sine functions (among them, 149 for the interaction region) are employed for the translational coordinate R_α in a range of $[0.015,15.0]a_0$. A total of 149 vibrational functions are employed for r_α in the range of [0.5,14.0] au for the reagent O_2 in the interaction region. We use $j_{max} = 120$ for the rotational basis. The permutation symmetry of the diatomic reagent is used, which saves half of the angular grid points. Full K blocks ($K_{max} = \min(J, j_{max})$) are used because, for the system, a rigorous treatment of Coriolis coupling is required. The time step used in the calculation is 10 au, and the total propagation time is 170000 au. The applied absorption potential starts from $r_\alpha = 10.8$ au and R_α=13.2 au. The dividing surface in the product region for extracting S-matrix information is placed at $R_{v0} = 10.5$ au. Only five PODVR points are used for r_v because there are only two open vibrational channels for the collision energy up to 1.5 eV. For rotational motion of the diatomic product, 22 Gaussian−Legendre quadrature points are employed. Thus, for each K_α block, we have in total 110 grid points on which the time-dependent wave function is evaluated during the wavepacket propagation. These 110 grid points are sufficient to converge product-state-resolved results up to $E_c = 1.5$ eV.

Figures 2 and 3 show the total reaction probabilities for the H + O_2 ($v_0 = 0, j_0 = 0$) reaction with $J = 0$ and 12, respectively, from the summation of the state-to-state reaction probabilities obtained by using the RCB approach, in comparison with those from the initial state-selected wavepacket (ISSWP) approach, which has been widely used for total reaction probability calculations in reactant Jacobi coordinates.[12−14,16,17,41] As can

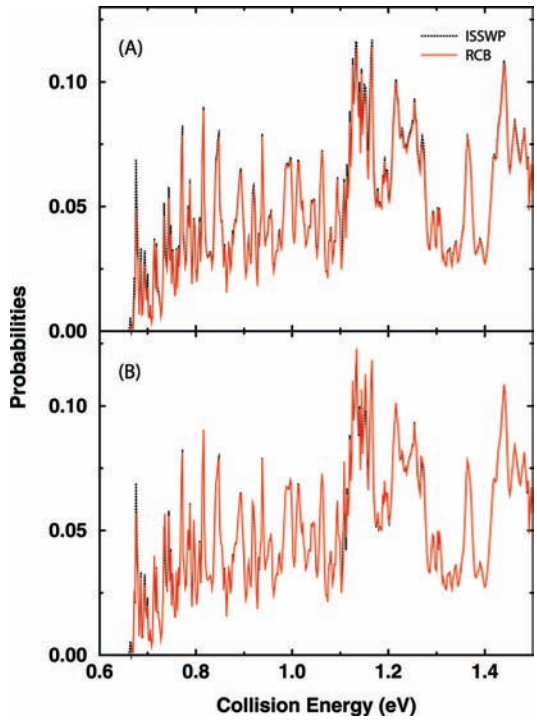

Figure 2. Total reaction probabilities for the H + O_2 ($v_0 = 0, j_0 = 0$) reaction for a total angular momentum of $J = 0$ obtained by using the RCB and ISSWP approaches. (A) The boundary matching is carried out at the matching point R_{v0} with the Riccati−Hankel function; (B) before performing boundary matching, the Riccati−Hankel function has been propagated by the renormalized Numerov method to the matching point R_{v0}.

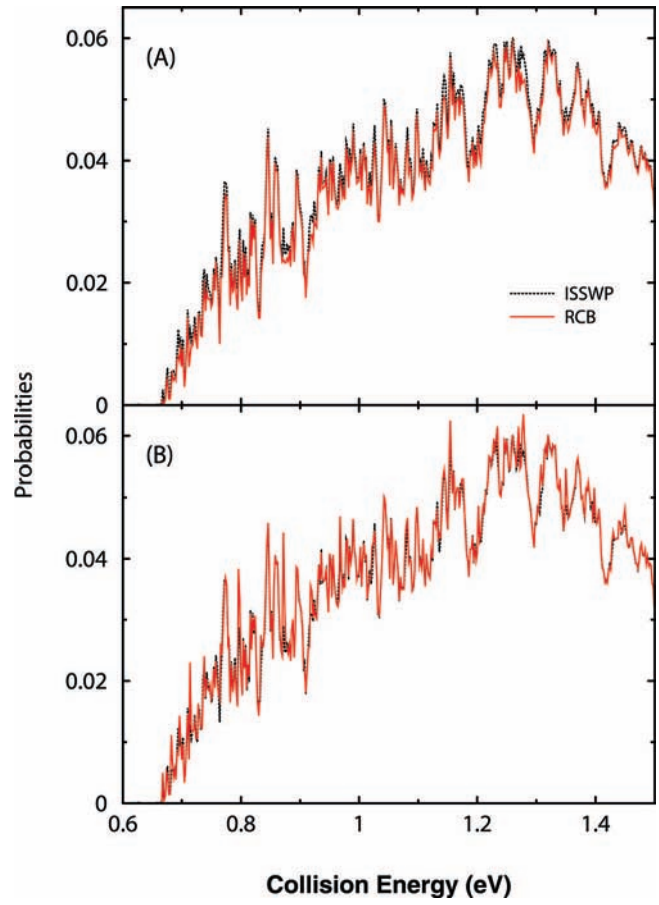

Figure 3. Same as Figure 2, except for $J = 12$.

be seen from Figures 2A and 3A, agreements between the total probabilities from the RCB and ISSWP calculations are very good, even without the renormalized Numerov propagation after the dividing surface, despite the fact that the total reaction probabilities are dominated by rich and sharp resonance structures. From Figures 2B and 3B, one can see that the renormalized Numerov propagation after the dividing surface does improve the accuracy of the total reaction probabilities, in particular, for $J = 12$ shown in Figure 3B. We found that for larger J, the renormalized Numerov propagation becomes even more important, indicating that the matching procedure becomes more sensitive to the residual long-range interaction after the dividing surface with an increasingly larger centrifugal interaction.

Figure 4 compares the vibrational-state-resolved reaction probabilities for the H + O_2 ($v_0 = 0, j_0$) → O + OH (v') reaction with a total angular momentum of $J = 0$ obtained by the present RCB method and by the PCB method implemented with coordinate transformation of the whole wavepacket in the interaction region.[8,30] First, we can see that vibrational-state-resolved reaction probabilities for the product HO ($v' = 0$) does not increase monotonously; instead, it begins to decrease with further increase of collision energy after the $v' = 1$ channel becomes open. As can be seen from the figure, the agreement is excellent between these two total different calculations, one using reactant Jacobi coordinates and the other using product Jacobi coordinates. This means that both approaches are able to provide sufficiently accurate dynamical information; what we should be concerned with is the computational efficiency. The numerical parameters for the PCB calculation to propagate the wavepacket in product Jacobi coordinates after coordinates transform are as follows. A total of 429 sine functions (among them, 269 for the interaction region) are employed for the translational coordinate R in a range of $[0.0,20.0]a_0$. A total of 119 vibrational functions are employed for r in the range of [0.5,13.0] au in the interaction region. We use $j_{max} = 140$ for the rotational basis. With these parameters, we can obtain well-converged state-to-state reaction probabilities for collision energies up to 1.5 eV. The time step used in the calculation is 10 au, and the total propagation time is 170000 au, as in the RCB calculations. The state-to-state analysis plane is placed at $R_v = 16.5$ au, which is sufficiently far to reach the true product asymptotic region with negligible interaction between O and OH. Hence, one can see that the numbers of basis functions for r and θ are quite close for these two calculations, while the number of basis functions for R coordinate used in the PCB calculation is almost double that used in the RCB calculation. Furthermore, the permutation symmetry of the diatomic reagent O_2 cannot be utilized in the product Jacobi coordinates, which increases the computational effort by more than a factor of 2. As a result, the computational time consumed for a PCB calculation is more than that required by the RCB approach by about a factor of 3, making it much harder to use the PCB approach to calculate DCS for this reaction.

Figure 5 shows rovibrational-state-resolved reaction probabilities for the product OH at the (j',v') = (0,0), (0,6), and (1,6) states, obtained by the PCB and RCB approaches for collision energies up to 1.5 eV and $J = 0$. Similar to the total reaction probabilities, the reaction probabilities to every product rotational state are dominated by narrow and mostly overlapping resonances. The reaction probabilities to the (0,0) and (0,6) states decrease very substantially in the high collision energy region, in particular, when the $v' = 1$ state becomes open. Again, one can see that the results from the PCB and RCB methods agree with each other very well. Since the dividing surface for S-matrix

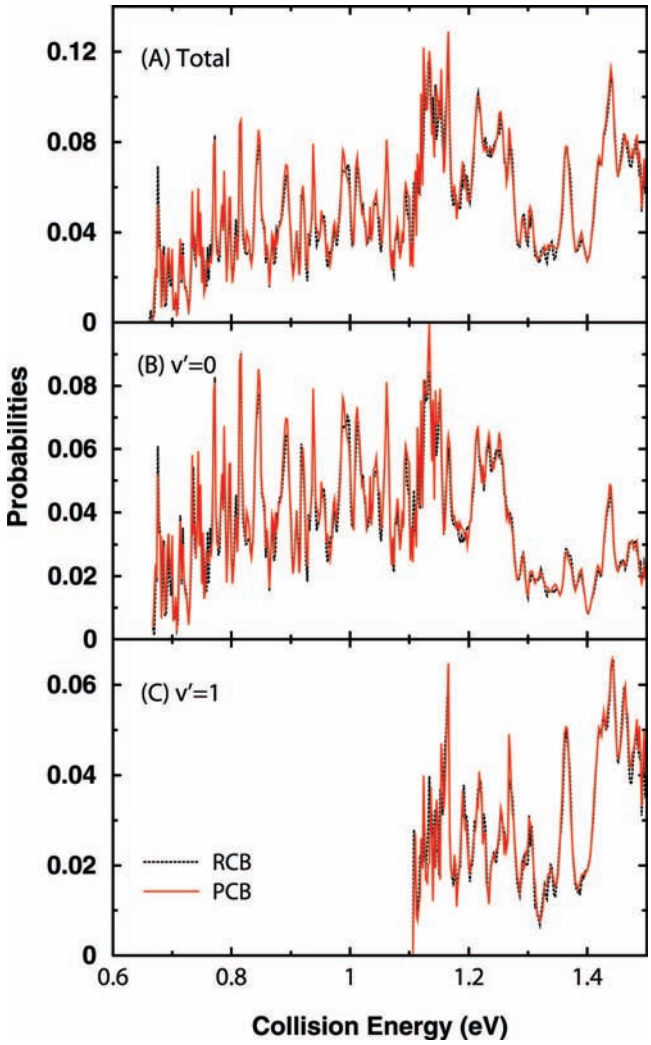

Figure 4. Vibrational-state-resolved reaction probabilities for the H + O_2 ($v_0 = 0, j_0 = 0$) → O + HO ($v' = 0,1$) reaction ($J = 0$) obtained by the RCB approach (black lines) and by the PCB approach (red lines). (A) Vibrational-state-resolved reaction probabilities summation (total reaction probabilities); (B) reaction probabilities for $v' = 0$; (C) reaction probabilities for $v' = 1$.

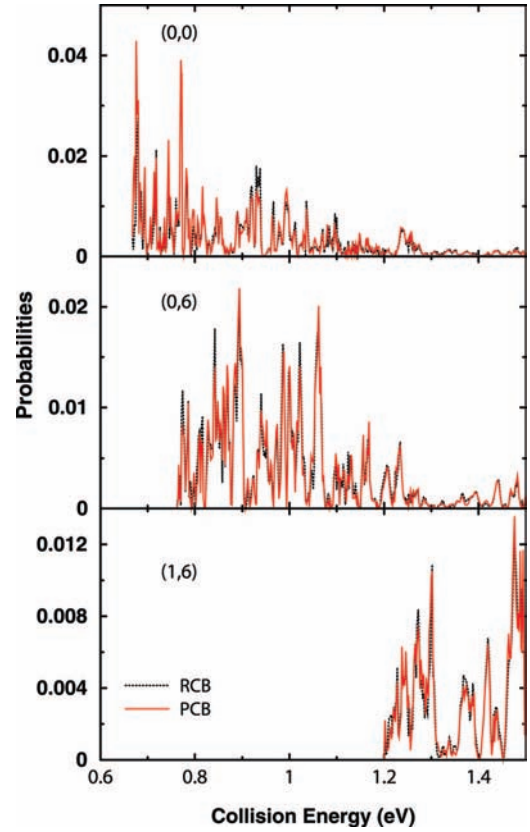

Figure 5. Rovibrational-state-resolved reaction probabilities for the H + O_2 ($v_0 = 0, j_0 = 0$) reaction ($J = 0$) to the product OH at the (j',v') = (0,0), (0,6), and (1,6) states, obtained by the PCB and RCB approaches as a function collision energy.

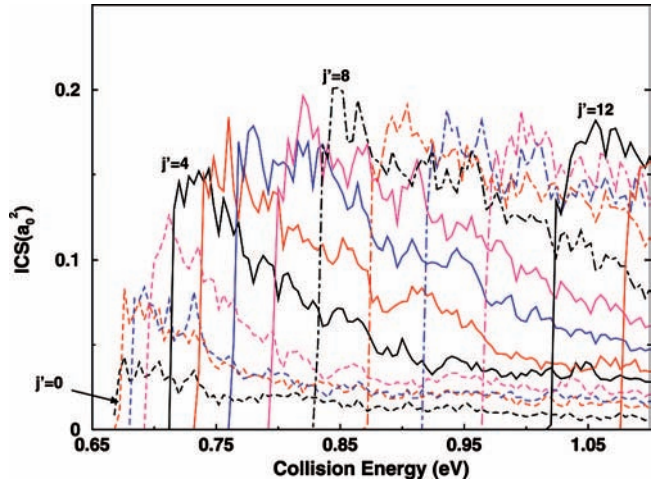

Figure 6. OH rotational-state-resolved integral cross sections as a function of collision energy, for the H + O_2 ($v_0 = 0, j_0 = 0$) reaction.

extraction in the PCB calculation is put at $R_{v0} = 16.5$ au, much further than that used in the RCB calculation of $R_{v0} = 10.5$ au, the good agreement between these two calculations on the rovibrational-state-resolved probabilities implies that the residual interaction potential after $R_{v0} = 10.5$ au does only have some elastic effects; hence, it is sufficiently accurate for us to extract the S matrix on the $R_{v0} = 10.5$ au dividing surface in our RCB calculation.

Calculations of the reactive cross sections for this reaction in a broad collision energy range are expensive computationally, even though the introduced RCB approach is very efficient for state-to-state study of the reaction. Besides the difficulties in the deep well description and rigorous Coriolis coupling consideration, a large number of partial waves should be included to converge the cross section because of the large collision energy threshold in the reactant channel and the heavy reduced mass of the system in the product channel. We calculated partial waves with J up to 52 to converge the cross section for a collision energy up to 1.1 eV. Figure 6 displays the rotational-state-resolved integral cross sections (ICS) for the H + O_2 ($v = 0, j = 0$) → O + OH ($v' = 0, j' = 0-13$) reaction with a collision energy up to 1.1 eV, right before the $v' = 1$ channel becomes open. As can be seen from the figure, ICS for every final rotational state increases very rapidly to its maximum value with the increase of the collision energy when the rotational state becomes open and then begins to decrease steadily with the further increase of the collision energy.

Figure 7 shows the rotational state distributions at collision energies of 0.7, 0.8, 0.9, and 1.0 eV for the (v_0, j_0) = (0,0) and (0,1) initial states. It is apparent that the distributions of the product rotational states from these two initial states are almost identical, indicating that the reaction dynamics is insensitive to the reagent rotational excitation, at least at low j_0 values. As

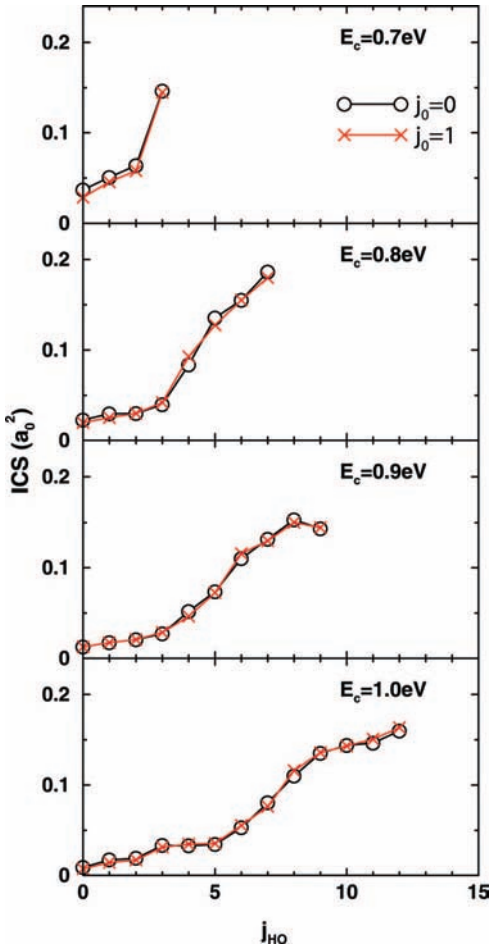

Figure 7. OH rotational-state-resolved integral cross sections for the H + O_2 ($v_0 = 0$, $j_0 = 0,1$) reactions at several collision energies.

we show in ref 59, the rotational state distribution increases almost monotonically with the rotational quantum number (j_{HO}) and peaks near the highest allowed rotational state, consistent with the complex-forming mechanism. However, the rotational state population does not increase linearly with j_{HO}; instead, it overpopulates at large j_{HO} values and underpopulates at small j_{HO} values. Hence, the OH rotational distribution is not fully statistical; otherwise, the population should increase linearly with j_{HO} because the number of rotational states increases linearly with j_{HO} due to the degeneracy factor. Such nonstatistical behaviors of OH rotational distributions[59] are consistent with earlier experimental observations.[79−81]

Figure 8 presents the ratio between the product rotational energy to the total available energy as a function of collision energy for the (v_0, j_0) = (0,0) initial state, along with the threshold energy of every rotational channel. As can be seen from the figure, about 50% of the total available energy is deposited on the rotational motion of OH, except in the very low energy region where the ratio has a smaller value. It is interesting to observe that the ratio curve exhibits oscillatory structure; once a rotational channel becomes open, there is a sharp rise in the ratio, indicating that this reaction has a strong preference to produce HO in the highest possible rotational states, as seen from rotational state distributions shown in Figure 7.

The differential cross sections (DCS) at collision energies of 0.7, 0.8, 0.9, and 1.0 eV are displayed in Figure 9 for initial states of (v_0, j_0) = (0,0) and (0,1). It is clear that the product angular distribution is dominated by scattering in both the

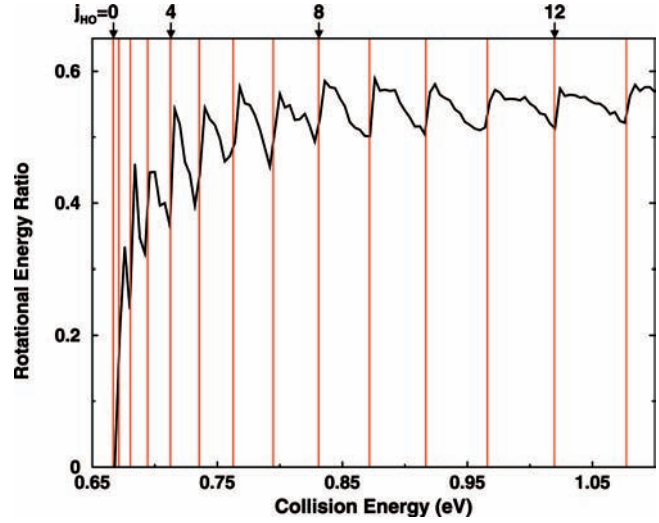

Figure 8. Fraction of total available energy deposited in the OH rotational energy as a function of the collision energy for the H + O_2 ($v_0 = 0$, $j_0 = 0$) reaction.

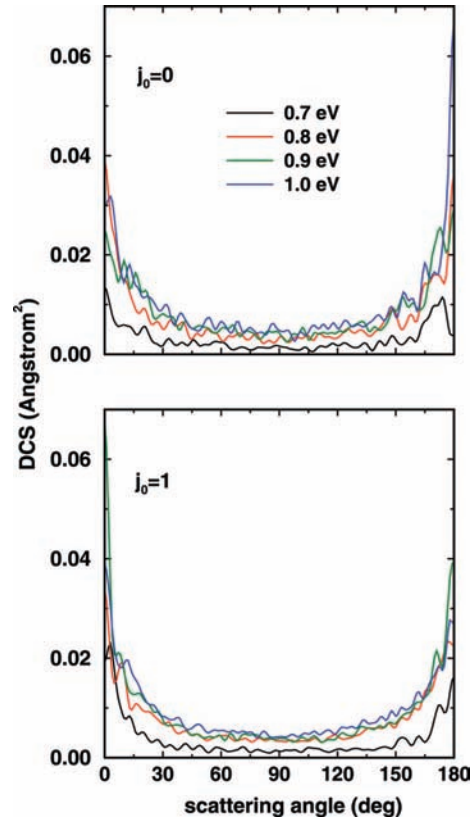

Figure 9. Differential cross sections for the H + O_2 ($v_0 = 0$, $j_0 = 0,1$) reactions at several collision energies.

forward and backward angles, again consistent with the complex-forming mechanism. However, the DCS are not entirely symmetrical, and the asymmetry varies with the collision energy. In addition, the DCS for $j_0 = 0$ and 1 show no qualitative difference, indicating again that the reaction dynamics is insensitive to the reagent rotational excitation, at least at low j_0 values.

4. Summary

We introduced a new time-dependent wavepacket method to study the A + BC → AB + C, AC+B reaction at the state-

to-state level. The method only requires propagating the wavepacket in the reactant Jacobi coordinates by extracting *S*-matrix information on a dividing surface right in front of the absorption potential. The method has particular advantages for reactions with deep wells and long-range attractive interactions in the product channels, in which the wavepacket in the product channels can only be absorbed sufficiently far away from the interaction potential. In addition, it is able to exploit the permutation symmetry of the reacting BC molecule if it contains two identical atoms or yield dynamical information for both the AB + C and AC + B channels from one wavepacket propagation if BC is a heteronuclear molecule. With an efficient way to obtain the product scattering wave functions represented in the reactant channel basis, the method is expected to be more efficient than the existing methods in dealing with systems with deep wells and long-range attractive interactions in the product channels and may find useful applications to many reactive scattering processes and to photodissociation dynamics processes where the product coordinates have a singularity problem.[82]

We first test this method on the $H + H_2$ reaction and obtain the state-to-state differential cross sections for collision energies up to 2.5 eV. The calculated DCS in low collision energy region are in excellent agreement with that obtained using the ABC code. For high collision energy, the current RCB method is much more efficient than the ABC program[4] in obtaining DCS. The method is further applied to the very challenging $H + O_2$ ($v_0 = 0, j_0 = 0,1$) reaction. DCS are obtained for the first time for collision energies up to 1.1 eV for the reaction. The calculations not only demonstrated the power and accuracy of the new RCB approach in dealing with complex-forming reactions but also shed light on the dynamics of the $H + O_2$ reaction.

Acknowledgment. We would like to thank Prof. Hua Guo and Prof. Daiqian Xie for many stimulated discussions and collaboration in the course of this work. The DICP group was supported by the Knowledge Innovation Program of the Chinese Academy of Science (Grants DICP R200402 and Y200601) and by the National Natural Science Foundation of China (Grant No. 20688301, 20773127). The NTU team was supported by a Singapore Ministry of Education Research Grant.

References and Notes

(1) Schatz, G. C.; Kuppermann, A. *J. Chem. Phys.* **1976**, *65*, 4642.
(2) Pack, R. T.; Packer, G. A. *J. Chem. Phys.* **1987**, *87*, 3888.
(3) Aquilanti, V.; Cavalli, S.; De Fazio, D. *J. Chem. Phys.* **1998**, *109*, 3792.
(4) Skouteris, D.; Castillo, J. F.; Manolopoulos, D. E. *Comput. Phys. Commun.* **2000**, *133*, 128.
(5) Honvault, P.; Launay, J.-M. *J. Chem. Phys.* **2001**, *114*, 1057.
(6) Althorpe, S. C. *J. Chem. Phys.* **2001**, *114*, 1601.
(7) Althorpe, S. C. *Nature* **2002**, *416*, 67.
(8) Yuan, K. J.; Cheng, Y.; Liu, X. H.; Harich, S.; Yang, X. M. *Phys. Rev. Lett.* **2006**, *96*, 103202.
(9) Lin, S. Y.; Guo, H. *Phys. Rev. A* **2006**, *74*, 022703.
(10) Gómez-Carrasco, S.; Roncero, O. *J. Chem. Phys.* **2006**, *125*, 054102.
(11) Hankel, M.; Smith, S. C.; Allan, R. J.; Gray, S. K.; Balint-Kurti, G. G. *J. Chem. Phys.* **2006**, *125*, 164303.
(12) Zhang, D. H.; Zhang, J. Z. H. *J. Chem. Phys.* **1994**, *101*, 1146.
(13) Zhang, D. H.; Light, J. C. *J. Chem. Phys.* **1996**, *104*, 4544.
(14) Yang, M.; Zhang, D. H.; Lee, S.-Y. *J. Chem. Phys.* **2002**, *117*, 9539.
(15) Zhang, D. H. *J. Chem. Phys.* **2006**, *125*, 133102.
(16) Wang, D. *J. Chem. Phys.* **2006**, *124*, 201105.
(17) Yang, M. *J. Chem. Phys.* **2008**, *129*, 064315.
(18) Harich, S. A.; Dai, D. X.; Yang, X. M.; Chao, S. D.; Skodje, R. T. *Nature* **2002**, *419*, 281.
(19) Dai, D. X.; Wang, C. C.; Harich, S. A.; Wang, X. Y.; Yang, X. M.; Chao, S. D.; Skodje, R. T. *Science* **2003**, *300*, 1730.
(20) Skodje, R. T.; Skouteris, D.; Manolopoulos, D. E.; Lee, S.-H.; Dong, F.; Liu, K. *Phys. Rev. Lett.* **2000**, *85*, 1206.
(21) Qiu, M. H.; Ren, Z. F.; Che, L.; Dai, D. X.; Harich, S. A.; Wang, X. Y.; Yang, X. M.; Xu, C. X.; Xie, D. Q.; Gustafsson, M.; Skodje, R. T.; Sun, Z. G.; Zhang, D. H. *Science* **2006**, *311*, 1440.
(22) Wang, X.; Dong, W.; Qiu, M.; Ren, Z.; Che, L.; Dai, D.; Wang, X.; Yang, X.; Sun, Z.; Fu, B.; Lee, S.-Y.; Xu, X.; Zhang, D. H. *Proc. Natl. Acad. Sci. U.S.A.* **2008**, *105*, 6227.
(23) Ren, Z.; Che, L.; Qiu, M.; Wang, X.; Dong, W.; Dai, D.; Wang, X.; Yang, X.; Sun, Z.; Fu, B.; Lee, S.-Y.; Xu, X.; Zhang, D. H. *Proc. Natl. Acad. Sci. U.S.A.* **2008**, *105*, 12662.
(24) Skouteris, D.; Manolopoulos, D. E.; Bian, W.; Werner, H.-J.; Lai, L.-H.; Liu, K. *Science* **1999**, *286*, 1913.
(25) Balucani, N.; Casavecchia, P.; Bañares, L.; Aoiz, F. J.; Gonzalez-Lezana, T.; Honvault, P.; Launay, J.-M. *J. Phys. Chem. A* **2006**, *110*, 817.
(26) Banares, L.; Castillo, J. F.; Honvault, P.; Launay, J.-M. *Phys. Chem. Chem. Phys.* **2005**, *7*, 627.
(27) Balucani, N.; Capozza, G.; Cartechini, L.; Bergeat, A.; Bobbenkamp, R.; Casavecchia, P.; Aoiz, F. J.; Banares, L.; Honvault, P.; Bussery-Honvault, B.; Launay, J.-M. *Phys. Chem. Chem. Phys.* **2004**, *6*, 4957.
(28) González-Lezana, T.; Roncero, O.; Honvault, P.; Launay, J.-M. *J. Chem. Phys.* **2006**, *125*, 094314.
(29) Honvault, P.; Lin, S. Y.; Xie, D. Q.; Guo, H. *J. Phys. Chem. A* **2007**, *111*, 5349.
(30) Fu, B.; Zhou, Y.; Zhang, D. H. *J. Theory Comput. Chem.* **2008**, *7*, 777.
(31) Peng, T.; Zhang, J. Z. H. *J. Chem. Phys.* **1996**, *105*, 6072.
(32) Peng, T.; Zhu, W.; Wang, D. Y.; Zhang, J. Z. H. *Faraday Discuss.* **1998**, *110*, 159.
(33) Dai, J. Q.; Zhang, J. Z. H. *J. Phys. Chem.* **1996**, *100*, 6898.
(34) Tannor, D. J.; Weeks, D. E. *J. Chem. Phys.* **1993**, *98*, 3884.
(35) Glassman, I. *Combustion*; Academic: New York, 1977.
(36) Miller, J. A.; Kee, R. J.; Westbrook, C. K. *Annu. Rev. Phys. Chem.* **1990**, *41*, 345.
(37) Jachimowski, I. *Combust. Flame* **1974**, *23*, 233.
(38) Smoot, L. D.; Hecker, W. C.; Williams, G. A. *Combust. Flame* **1976**, *26*, 323.
(39) Pastrana, M. R.; Quintales, L. A. M.; Brandao, J.; Varandas, A. J. C. *J. Phys. Chem.* **1990**, *94*, 8073.
(40) Varandas, A. J.C.; Brandao, J.; Pastrana, M. R. *J. Chem. Phys.* **1992**, *96*, 5137.
(41) Zhang, D. H.; Zhang, J. Z. H. *J. Chem. Phys.* **1994**, *101*, 3671.
(42) Pack, R. T.; Butcher, E. A.; Packer, G. A. *J. Chem. Phys.* **1995**, *102*, 5998.
(43) Miller, J. A.; Garrett, B. C. *Int. J. Chem. Kinet.* **1997**, *29*, 275.
(44) Meijer, A. J. H. M.; Goldfield, E. M. *J. Chem. Phys.* **1998**, *108*, 5404.
(45) Goldfield, E. M.; Meijer, A. J. H. M. *J. Chem. Phys.* **2000**, *113*, 11055.
(46) Teitelbaum, H.; Caridade, P. J. S. B.; Varandas, A. J. C. *J. Chem. Phys.* **2004**, *120*, 10483.
(47) Dochovic, R. J.; Parker, M. A. *J. Phys. Chem. A* **2005**, *109*, 5883.
(48) Bargeuno, P.; Goonzalez-Lenzana, T.; Larregaray, P.; Bonnet, L.; Rayez, J. *Phys. Chem. Chem. Phys.* **2007**, *9*, 1127.
(49) Harding, L. B.; Troe, J.; Ushakov, V. G. *Phys. Chem. Chem. Phys.* **2000**, *2*, 631.
(50) Harding, L. B.; Maergoiz, A. I.; Troe, J.; Ushakov, V. G. *J. Chem. Phys.* **2000**, *113*, 11019.
(51) Sultanov, R. A.; Balakrishnan, N. *J. Phys. Chem. A* **2004**, *108*, 8759.
(52) Abu Bajeh, M.; Goldfield, E. M.; Hanf, A.; Kappel, C.; Meijer, A. J. H. M.; Volpp, H.; Wolfrum, J. *J. Phys. Chem. A* **2001**, *105*, 3359.
(53) Xu, C. X.; Zhang, D. H.; Xie, D. Q.; Lin, S. Y.; Guo, H. *J. Chem. Phys.* **2005**, *122*, 244305.
(54) Lin, S. Y.; Xie, D.; Guo, H. *J. Chem. Phys.* **2006**, *125*, 091103.
(55) Xu, C.; Jiang, B.; Xie, D.; Farantos, S. C.; Lin, S. Y.; Guo, H. *J. Phys. Chem. A* **2007**, *111*, 10353.
(56) Lin, S. Y.; Guo, H.; Honvault, P.; Xie, D. *J. Phys. Chem. B* **2006**, *110*, 23641.
(57) Lin, S. Y.; Rackham, E. J.; Guo, H. *J. Phys. Chem. A* **2006**, *110*, 1534.
(58) Hankel, M.; Smith, S. C.; Meijer, A. J. H. M. *J. Chem. Phys.* **2007**, *127*, 064316.
(59) Sun, Z.; Zhang, D. H.; Xu, C.; Zhou, S.; Xie, D.; Lendvay, G.; Lee, S.-Y.; Lin, S. Y.; Guo, H. *J. Am. Chem. Soc.* **2008**, *130*, 114319.
(60) Echave, J.; Clary, D. C. *Chem. Phys. Lett.* **1992**, *190*, 225.
(61) Feit, M. D.; Fleck, J. A., Jr.; Steiger, A. *J. Comput. Phys.* **1982**, *47*, 412.
(62) Fleck, J. A., Jr.; Morris, J. R.; Feit, M. D. *Ann. Phys.* **1976**, *10*, 129.
(63) Zhang, D. H.; Zhang, J. Z. H. *J. Chem. Phys.* **1993**, *99*, 5615.
(64) Zhang, D. H.; Zhang, J. Z. H. *J. Chem. Phys.* **1994**, *100*, 2697.
(65) Zhang, D. H.; Zhang, J. Z. H. *J. Chem. Phys.* **1994**, *100*, 5631.

(66) Fu, B.; Zhang, D. H. *J. Phys. Chem. A* **2007**, *111*, 9516.
(67) Brink, D. M.; Satchler, G. R. *Angular Momentum*, 2nd ed.; Clarendon, Oxford, U.K., 1968.
(68) Yang, W. T.; Peet, A. C. *Chem. Phys. Lett.* **1988**, *153*, 98.
(69) Zhang, J. Z. H. *J. Chem. Phys.* **1991**, *94*, 6047.
(70) Zare, R. N. *Angular Momentum*; Wiley: New York, 1988.
(71) Zhang, J. Z. H.; Miller, W. H. *J. Chem. Phys.* **1989**, *91*, 1528.
(72) Rackham, E. J.; Gonzalez-Lezana, T.; Manolopoulos, D. E. *J. Chem. Phys.* **2003**, *119*, 12895.
(73) Quéméner, G.; Honvault, P.; Launay, J. M. *Phys. Rev. A* **2005**, *71*, 032772.
(74) Aoiz, F. J.; Bañares, L.; Herrero, V. J. *Int. Rev. Phys. Chem.* **2005**, *24*, 119.
(75) Banares, L.; Aoiz, F. J.; Herrero, V. J.; D'Mello, M. J.; Niederjohann, B.; Seekamp-Rahn, K.; Wrede, E.; Schnieder, L. *J. Chem. Phys.* **1998**, *108*, 6160.
(76) Boothroyd, A. I.; Keogh, W. J.; Martin, P. G.; Peterson, M. R. *J. Chem. Phys.* **1996**, *104*, 7139.
(77) Mielke, S. L.; Garrett, B. C.; Peterson, K. A. *J. Chem. Phys.* **2002**, *116*, 4142.
(78) Mielke, S. L.; Peterson, K. A.; Schwenke, D. W.; Garret, B. C.; Truhlar, D. G.; Michael, J. V.; Su, M.-C.; Sutherland, J. W. *Phys. Rev. Lett.* **2003**, *91*, 063201.
(79) Bronikowski, M. J.; Zhang, R.; Rakestraw, D. J.; Zare, R. N. *Chem. Phys. Lett.* **1989**, *156*, 7.
(80) Kleinermanns, K.; Linnebach, E.; Pohl, M. *J. Chem. Phys.* **1989**, *91*, 2181.
(81) Kleinermanns, K.; Linnebach, E. *J. Chem. Phys.* **1985**, *82*, 5012.
(82) Lepetit, B.; Lemoine, D. *J. Chem. Phys.* **2002**, *117*, 8676.

JP810512J